ELSEVIER

PII: S0141-0296(96)00154-X

Engineering Structures, Vol. 19, No. 9, pp. 748–759, 1997

0141-0296/97 $17.00 + 0.00

Experimental study of prefabricated funicular shell units

Abolhassan Vafai, Massoud Mofid and Homayoon E. Estekanchi

Department of Civil Engineering, Sharif University of Technology, Tehran, Iran
(Received April 1994; revised version accepted June 1995)

The experimental values of membrane stresses in the elastic range along diagonal sections of funicular shell structures are calculated and compared with the theory. The results are generally found to be in close agreement with the theory. Experimental values of vertical deflections along the longitudinal and transverse sections of the shells also compare favorably with the theory. The experimental failure and crack loads are found and empirical equations, expressing the relation between rise and failure and crack loads, are given.

Keywords: funicular shells, experimental investigation, prefabricated shell units

Introduction

Shell structures are widely used in the fields of civil, mechanical, architectural and marine engineering. Shell technology has been enhanced by the development of new materials and prefabrication schemes, and shells of various types and forms have been known to display high potential in the fields of prefabricated shell construction. Shell units of a variety of dimensions and sizes have been constructed in metal, concrete and composite materials for many different structural purposes. The efficiency of these units and their suitability for use in prefabricated construction arises from the fact that shells are usually lighter, when constructed in a controlled area and mass produced, are more economical and, from the aesthetic point of view, are considered superior when compared to other types of structural shapes[1–6].

The behavior of prefabricated shell units has been investigated, both theoretically and experimentally, by many researchers[1,4,7–10]. Apart from construction schemes, the use of prefabricated shell units creates certain problems which have to be investigated from the research point of view. One of the most important is the structural behavior of the units when subjected to the concentrated loads at various points along their span. Another consideration of interest is the ultimate strength and the pattern of failure for these types of shells. The shells of double curvature usually offer a higher ultimate strength than the shells of single curvature, such as cylindrical shells[2]. The problem of prefabricated shells of double curvature, subjected to concentrated load and supported at two edges, has previously been investigated by the principal author[1]. In practice there are cases in which these shells are supported on four edges, however, a survey of the related literature reveals that not much research has been done in this area.

This paper contains the results of numerical and experimental studies carried out in the area of funicular shell units with square bases supported at four edges and subjected to concentrated loading at the apex. A particular design is given for the geometry, the form, the rise and the type of reinforcement of the units. Forty-five models are constructed based on this design. First, eight samples supported at four edges are loaded to a specified load within the elastic region. Electrical resistance gauges are mounted both inside and outside at several locations along the diagonal on the surface of the shell on two different specimens with a rise of 6 and 9 cm, respectively. Also, dial gauges are installed at several locations on the surface of the other six specimens with varying rise and reinforcement types. Following these non-destructive tests, all 45 samples are loaded to failure, subjected to concentrated load at the centre. To relate experimental results to theory, the finite-element technique (SAP90 Program) is utililized to analyse a similar model in the elastic range.

Problem theory

In general, the equation of a doubly curved funicular surface, with in-plane rectangular edges formed by the application of a uniform surface pressure, can be presented in the form:

$$z = f(x, y) \tag{1}$$

In this shape, it is possible to assume a desired state of stress under a specified condition of loading (*Figure 1*). The idea in design and construction of this type of funicular shell is that the tensile stress does not develop. This basic assumption leads to a 'fully compressive stress optimal design' of this funicular surface[3].

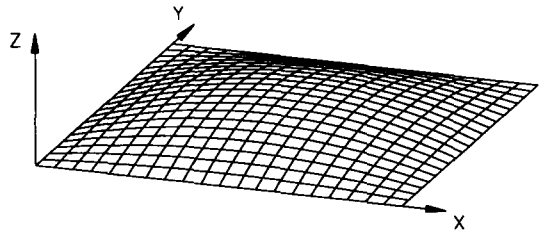

Figure 1 Funicular surface with rectangular in-plane edges (deformed shape under uniform vertical pressure)

Equation (1), which represents the shape of a funicular surface under a specified downward vertical loading per unit area, could be found analytically in a series form. However, a closed form solution of this equation, for the type of surface under general loading, is not available.

Funicular shape

To develop a funicular surface, with a specified state of stress, one must first consider an element of doubly-curved shell and its projection on a horizontal plane, as shown in *Figure 2*.

The projected stresses $[\bar{N}_x, \bar{N}_y, (\bar{N}_{xy} = \bar{N}_{yx})]$ and loadings, (X, Y, Z) are related to the real stresses $[N_x, N_y, (N_{xy} = N_{yx})]$ and loadings (F_x, F_y, F_z), respectively, in the following manner[4]:

$$\bar{N}_x = N_x[(1 + q^2)/(1 + p^2)]^{1/2} \tag{2a}$$

$$\bar{N}_y = N_y[(1 + p^2)/(1 + q^2)]^{1/2} \tag{2b}$$

$$\bar{N}_{xy} = N_{xy} \tag{2c}$$

$$\bar{X} = F_x[(1 + p^2 + q^2)]^{1/2} \tag{3a}$$

$$\bar{Y} = F_y[(1 + p^2 + q^2)]^{1/2} \tag{3b}$$

$$\bar{Z} = F_z[(1 + p^2 + q^2)]^{1/2} \tag{3c}$$

where

$$p = \frac{\partial z}{\partial x} \tag{4a}$$

$$q = \frac{\partial z}{\partial y} \tag{4b}$$

For a general loading, on a general double-curved shell element, the equilibrium in the z-direction may be written as:

$$\bar{N}_x \frac{\partial^2 z}{\partial x^2} + 2\bar{N}_{xy} \frac{\partial^2 z}{\partial x \partial y} + \bar{N}_y \frac{\partial^2 z}{\partial y^2} = \bar{Q} \tag{5}$$

where: $\bar{Q} = -\bar{Z} + p\bar{X} + q\bar{Y}$ = general loading.

There is no closed form solution for Eq. (5). However, for a vertical downward loading per unit area ($X = Y = 0$) and thin shallow doubly curved shell element with small curvature:

$$\frac{\partial z}{\partial x} = \frac{\partial z}{\partial y} \approx 0 \tag{6}$$

Equation (5) can be simplified in the following form:

$$\bar{N}_x \approx N_x \tag{7a}$$

$$\bar{N}_y \approx N_y \tag{7b}$$

$$\bar{Q} = -F_z = -q \tag{7c}$$

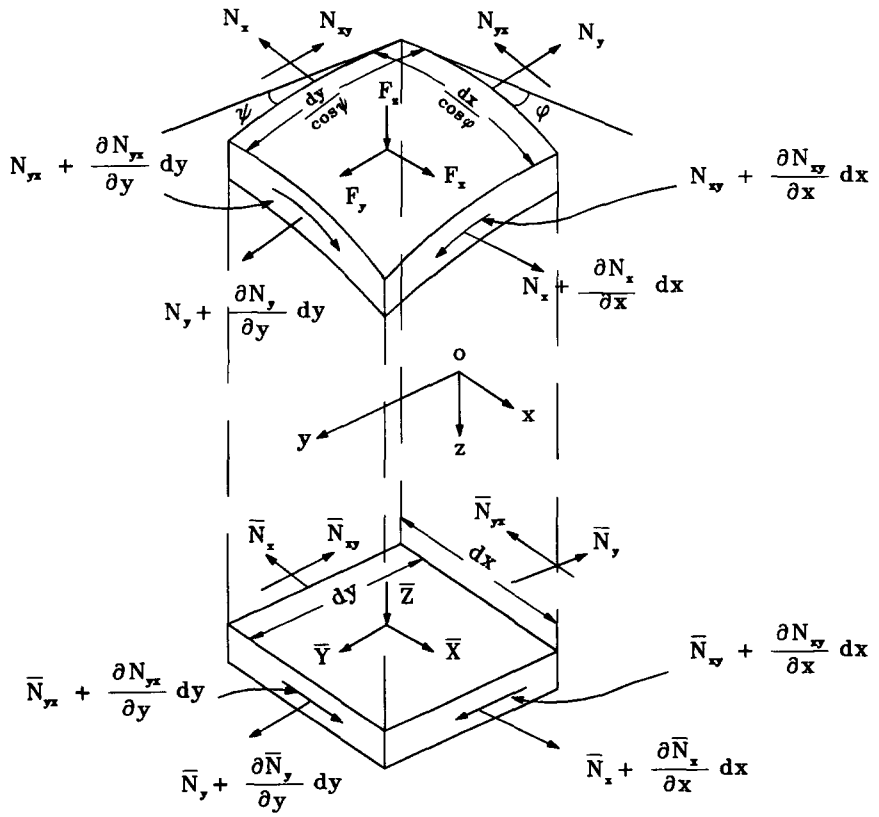

Figure 2 Doubly curved shell element and its projection on *XY* plane

$$\because N_x \frac{\partial^2 z}{\partial x^2} + 2N_{xy} \frac{\partial^2 z}{\partial x \partial y} + N_y \frac{\partial^2 z}{\partial y^2} = -q \quad (8)$$

A funicular shell with a specified state of stress as discussed in Eq. (8), can be written in the form:

$$N_x = N_y = -N \text{ (allowable compression stress)} \quad (9a)$$

$$N_{xy} = 0 \quad (9b)$$

$$\frac{\partial^2 z}{\partial x^2} + \frac{\partial^2 z}{\partial y^2} = \frac{q}{N} \quad (10a)$$

or

$$\nabla^2 z = \frac{q}{N} \quad (10b)$$

Equation (10) for a square base funicular shell, has a solution in a series form[4]:

$$z_0 = \frac{16ga^2}{N\pi^3} \sum_{n=1,3,5}^{\infty} (-1)^{\frac{n-1}{2}} \times \frac{1}{n^3} \times \left(1 - \frac{\cosh(n\pi y/2a)}{\cosh(n\pi/2)}\right) \cos \frac{n\pi x}{2a} \quad (11)$$

where z_0 = height measured from the base; g = acceleration of gravity; N = constant membrane stress in the shell, and a = base dimension (of both sides). The surface generated by this equation is graphically presented in *Figure 1*.

Construction of shell specimens

An apparatus consisting of a double-edge steel frame and a cloth membrane was used to build the specimens. The membrane was stretched within the boundaries of the frame and clamped therein. The amount of stretching depended on the desired rise of the shell units. Three centimeters of concrete were poured into the prepared forming system, the resultant sag due to the weight of concrete would cause the membrane to stretch and deflect, thus making the final form in the shape of the stretched membrane with the desired rise. The specimens constructed can be considered a funicular shell, which, under described loading, would undergo internal membrane forces with negligible bending effect[2].

All shells were moist cured for at least 28 days before testing. A total of 45 specimens were constructed, with a constant edge dimension ($2a$) of 100 cm with varying rises (h) 5–9 cm and 9.50 mm in diameter steel bars placed in the corner near the edges of the diaphragm. Referring to *Figure 3*, the following equation, which is an approximate form of Eq. (11), is used to describe the surface of funicular shell over a square ground plan[4].

$$z_{0(x,y)} = h\left(1 - \frac{(x-a)^2}{a^2}\right)\left(1 - \frac{(y-a)^2}{a^2}\right) \quad (12)$$

where h = height at shell center; x, y = in-plane shell coordinates at which z_0 is to be calculated. The other terms in Eq. (12) have been previously defined.

From the 45 specimens constructed, 15 had no surface reinforcement, 15 used a wire mesh (ordinary chicken wire) through the middle surface which was connected to the edge diaphragm rebars, and the last 15 had wire reinforcement made from mild steel wire from a fiber size of 0.016 in (0.4 mm) × 1.00 in (2.5 mm). The content of fiber wire was 2% of the volume.

The shell units were constructed using ordinary Portland cement and fine natural sand aggregate. The particulars of mix design are shown in *Table 1*. *Figure 4* shows the geometry as well as the detail of the reinforcement of the three different shell units. The reinforcement has been labeled as Types I, II and III in *Figure 4*. Specifications of the shell specimens are given in *Table 2*.

Finite-element model

To relate experimental results with theory, a numerical study was conducted. The model consisted of a funicular shell loaded at its apex. The finite-element technique and a related computer program (SAP 90) were utilizied to analyse the structure. Shell elements are 4-node membrane and

Table 1 The particulars of the mix design

Portland cement	512 kg/m³ (32 lb/ft³)
Coarse aggregate	608 kg/m³ (38 lb/ft³)
Fine sand	1055 kg/m³ (66 lb/ft³)
Water/cement ratio	0.43
Unit weight	23.5 kN/m³ (150 lb/ft³)
Ultimate compressive strength	34.3 × 10⁶ Pa (5480 psi)
Modulus of elasticity	17.8 × 10⁹ Pa (2580 ksi)
Poisson's ratio	0.2

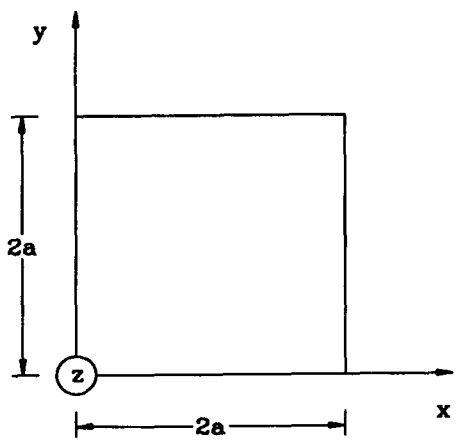

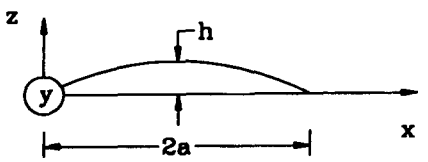

Figure 3 Funicular shell coordinate system

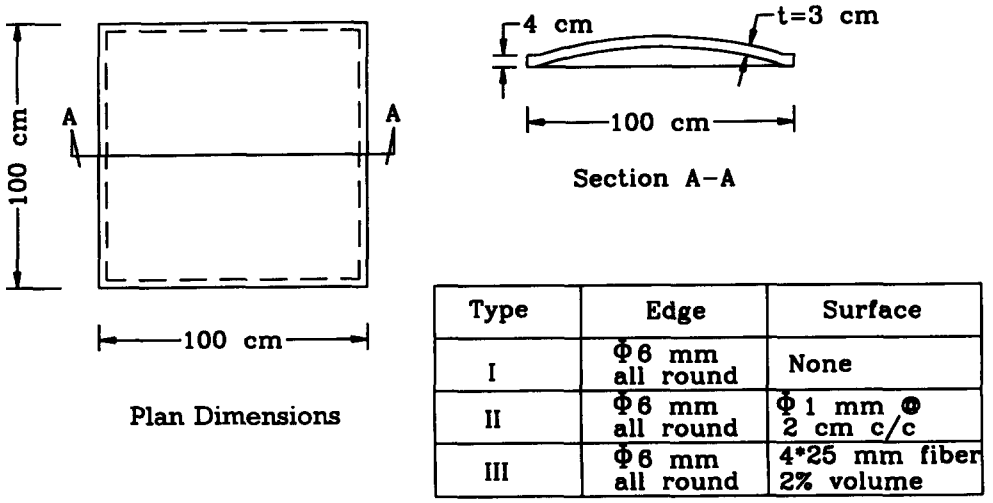

Figure 4 Geometry and details of reinforcement types

Table 2 Specifications of the shell specimens

No.	Specimen designation	Rise (cm)	Reinf. type*	No.	Specimen designation	Rise (cm)	Reinf. type*	No.	Specimen designation	Rise (cm)	Reinf. type*
1	S511	5	I	16	S521	5	II	31	S531	5	III
2	S512	5	I	17	S522	5	II	32	S532	5	III
3	S513	5	I	18	S523	5	II	33	S533	5	III
4	S611**	6	I	19	S621**	6	II	34	S631**	6	III
5	S612***	6	I	20	S622	6	II	35	S632	6	III
6	S613	6	I	21	S623	6	II	36	S633	6	III
7	S711	7	I	22	S721	7	II	37	S731	7	III
8	S712	7	I	23	S722	7	II	38	S732	7	III
9	S713	7	I	24	S723	7	II	39	S733	7	III
10	S811	8	I	25	S821	8	II	40	S831	8	III
11	S812	8	I	26	S822	8	II	41	S832	8	III
12	S813	8	I	27	S823	8	II	42	S833	8	III
13	S911**	9	I	28	S921**	9	II	43	S931**	9	III
14	S912***	9	I	29	S922	9	II	44	S932	9	III
15	S913	9	I	30	S923	9	II	45	S933	9	III

*Reinforcement types are as in *Figure 4*
**Instrumented with dial gauges
***Instrumented with strain gauges

plate bending elements[11]. The plan of the shell, its dimensions, and the finite-element mesh consisting of 400 elements, 5 × 5 cm each, is shown in *Figure 5*. The finite-element model used to analyse the shell is based on the assumption that the material is linearly elastic. Hence, the numerical results are expected to be valid only in the elastic region of shell behavior. The effect of surface reinforcement in this linear elastic model may be approximated by a smearing approach, in which the elastic modulus of the shell material is increased by an appropriate amount. However, since the instrumented specimens had no surface reinforcement, the modulus of elasticity of plane concrete was used as an effective modulus.

Tables 3 and *4* show membrane forces and deflections along sections AA and BB, respectively. This analysis has been carried out for a shell of double curvature with a thickness of 3 cm and subjected to a concentrated load of 10 KN at the centre of the specimen. The difference in the element forces calculated from the different elements attached to a common joint, is less than 3% of the element force. This can be considered as an estimate of approximate error in the element forces. The convergence of the solution was also assessed by comparing the results of this analysis with another one, obtained using a coarser mesh. Little difference was revealed, indicating that a convergent solution was reached.

Instrumentation and testing

To investigate the behavior of the funicular shell subjected to a concentrated load at its apex, the structure was instrumented and loaded as follows: two specimens with a rise of 6 and 9 cm, respectively, were chosen for strain measurement. Electrical resistance strain gauge rosettes were mounted on the top and bottom surfaces of the two shells (S612 and S912), at the lower left corner along the diagonal of each shell at three different locations. Six specimens, with different reinforcements and rises, were used for dial gauge readings. *Tables 5* and *6* show the location of strain gauges as well as installed dial gauges. *Figures 6* and *7* show the instrumented specimens and the installed dial gauge specimens, respectively.

The shell units, with varying rises and different types of reinforcement, were placed in a loading apparatus designed for this purpose, as shown in *Figure 8*. To check the elastic behavior of the shells, the structures were loaded and

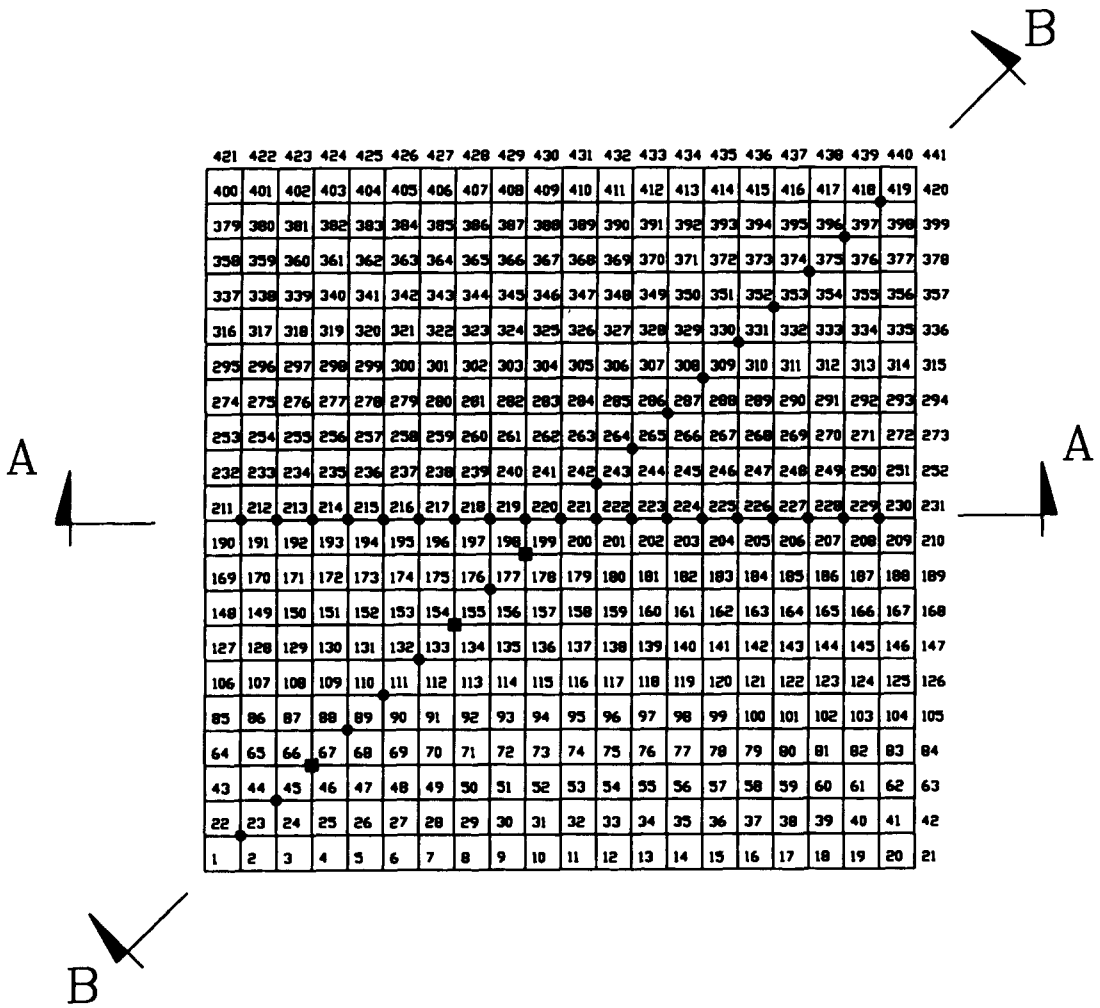

Figure 5 Finite-element model and corresponding node numbers

Table 3 Shell forces per unit length for concentrated load of 10 kN along sections A–A and B–B

Node no	*X*-coord. cm	*Y*-coord. cm	Rise = 6 cm			Rise = 9 cm		
			N_x N/cm	N_y N/cm	N_{xy} N/cm	N_x N/cm	N_y N/cm	N_{xy} N/cm
1	0	0	0.09	0.09	0.06	0.19	0.18	0.12
23	5	5	−48.78	−48.71	−27.97	−41.68	−41.53	−24.92
45	10	10	−67.87	−67.54	−39.34	−52.80	−52.11	−36.59
67	15	15	−83.87	−83.12	−54.97	−54.88	−53.17	−55.73
89	20	20	−104.81	−103.56	−76.90	−56.13	−53.05	−84.97
111	25	25	−142.13	−140.54	−100.53	−70.95	−66.78	−118.69
133	30	30	−208.23	−206.71	−117.14	−117.65	−113.44	−145.67
155	35	35	−312.57	−311.53	−117.16	−214.43	−211.41	−152.43
177	40	40	−456.02	−455.57	−93.77	−371.80	−370.43	−127.28
199	45	45	−621.61	−621.09	−47.97	−577.34	−576.00	−67.94
221	50	50	−735.11	−735.11	−4.22	−731.26	−731.25	−6.29
212	5	50	−25.48	−327.62	4.43	4.04	−198.68	4.89
213	10	50	−7.91	−351.91	5.38	34.28	−224.99	6.03
214	15	50	−10.16	−380.58	4.43	50.35	−258.22	5.04
215	20	50	−37.66	−416.08	2.13	43.12	−301.27	2.41
216	25	50	−96.42	−459.69	−1.18	2.09	−355.99	−1.60
217	30	50	−190.78	−511.73	−5.21	−82.66	−423.19	−6.76
218	35	50	−320.76	−571.07	−9.47	−217.38	−501.92	−12.60
219	40	50	−477.93	−635.02	−12.68	−398.44	−589.14	−17.38
220	45	50	−637.88	−699.32	−17.89	−599.54	−679.67	−25.77

Table 4 Vertical displacements for a concentrated load of 10 kN along sections A–A and B–B

Node No.	*X*-coord cm	*Y*-coord cm	Rise = 6 cm U_z (cm)	Rise = 9 cm U_z (cm)
23	5	5	–0.00004	0.00002
45	10	10	–0.00016	0.00013
67	15	15	–0.00054	0.00031
89	20	20	–0.00167	0.00025
111	25	25	–0.00428	–0.00063
133	30	30	–0.00918	–0.00315
155	35	35	–0.01705	–0.00818
177	40	40	–0.02791	–0.01624
199	45	45	–0.04036	–0.02656
221	50	50	–0.04889	–0.03429
212	5	50	–0.00054	–0.00061
213	10	50	–0.00164	0.00078
214	15	50	–0.00371	0.00015
215	20	50	–0.00708	–0.00154
216	25	50	–0.01194	–0.00450
217	30	50	–0.01835	–0.00893
218	35	50	–0.02621	–0.01483
219	40	50	–0.03501	–0.02196
220	45	50	–0.04366	–0.02947

Figure 6 Instrumented shell specimen

unloaded several times. Of these, the two instrumented shells, with 6 cm and 9 cm rise, respectively, were loaded concentrically at the apex in the elastic range. Strain gauge readings were recorded at six different load increments. The results are presented in *Tables 7–12*.

Deflection measurements were also carried out for shells

Table 5 Location of strain gauges

Rise	Type of reinforcement	Location	Node No.	*X*-coordinate cm	*Y*-coordinate cm
6 cm	I	I bottom	67	15	15
		I top	67	15	15
		II bottom	155	35	35
		II top	155	35	35
		III bottom	199	45	45
		III top	199	45	45
9 cm	I	I bottom	67	15	15
		I top	67	15	15
		II bottom	155	35	35
		II top	155	35	35
		III bottom	199	45	45
		III top	199	45	45

Table 6 Location of dial gauges

Rise cm	Type of reinforcement	Gauge No.	Corresponding node No.	*X*-coordinate cm	*Y*-coordinate cm
6	I, II, IIII	1	213	10	50
		2	215	20	50
		3	217	30	50
		4	219	40	50
		5	45	10	10
		6	—	21	21
		7	—	32	32
		8	155	35	35
		9	—	42.5	42.5
		10	—	44	44
9	I, II, III	1	213	10	50
		2	215	20	50
		3	217	30	50
		4	219	40	50
		5	45	10	10
		6	—	21	21
		7	—	32	32
		8	111	25	25
		9	—	42.5	42.5
		10	—	44	44

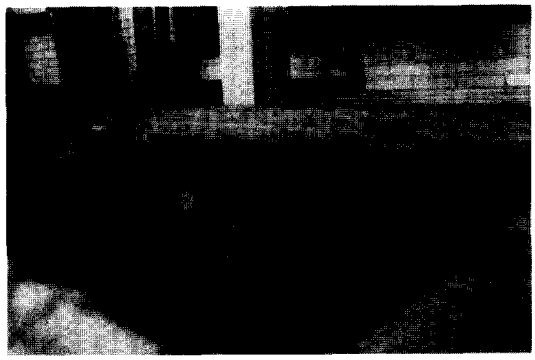

Figure 7 Installed dial gauges on test specimen

Figure 8 Instrumented specimen subjected to concentrated loading

with different rises, namely 6 and 9 cm, as shown in *Tables 13* and *14*.

To investigate the ultimate strength of each shell, all 45 specimens were loaded to failure and the corresponding crack and failure loads were recorded and presented in *Tables 15–17*.

Results and conclusions

Forty-five funicular shells were constructed, loaded concentrically and tested as described. From the results of testing two different specimens with a rise of 6 and 9 cm, respectively, instrumented with strain gauges, the values of strains for different loadings were recorded. The average strains, both on the inside and outside surfaces of the shells at three different locations, for six different loading increments within the elastic region along the diagonal, were measured and the results are presented in *Tables 7–12*. Using Hook's law and the Mohr circle, the experimental values of membrane forces per unit length (N_1 and N_2) were calculated and the results are presented in *Tables 7–12* along with numerical values using finite-elements method. The calculated principal stresses were plotted, along with the numerical values in *Figures 9* and *10*. The comparison of the results for both shells (6 cm and 9 cm in rise), shows, in general, for three locations, the experimental values to be within 12% of the FE analysis. The comparison of the results shows that the difference between theoretical and experimental is less in the middle than in the regions close to boundary and the location of concentrated load. This could be attributed to the disturbance caused by boundary and concentrated load.

Another set of curves were constructed, as shown in *Figures 11–14*, to show the numerical and normalized experimental values of vertical deflections along sections A–A and B–B of the tested shells. These curves are plotted for different types of reinforcements. The comparison of the two results indicates that at most locations the numerical yields lower values than the experimental. The discrepancies between the finite-element approach and the experiment could be attributed to possible errors associated with experimental procedure. However, the overall patterns of deflection in both numerical and experimental are identical. The results also indicate, as expected, that the inclusion of reinforcement has a stiffening effect on the shells. The figures show that of the three different reinforcement types used in this experiment, shells with wire mesh reinforcement exhibit the least deflection, while shells with no surface reinforcement have the most deflections.

To investigate the ultimate strength of the shells, all 45 specimens were loaded to complete rupture. *Tables 15–17* show the load at which initial cracks occurred for each specimen and the failure load of each unit as it is related to rise and type of reinforcement. It was observed that, invariably, the cracks initiated at and around the centre nearest to the point of the application of the concentrated

Table 7 Experiment and theoretical results for specimen with 9 cm rise at location I

		Load (N)					
Strain (cm/cm)		1110	2230	3340	4450	5560	6680
$\epsilon_x \times 10^6$		−0.50	−1.50	−3.00	−4.00	−4.50	−6.50
$\epsilon_y \times 10^6$		−1.83	−3.17	−3.00	−4.67	−5.17	−6.17
$\epsilon_{xy} \times 10^6$		3.46	5.20	9.24	12.70	15.01	17.90
		Force per unit length (N/cm)					
N_x	Exp.	−4.83	−11.88	−20.04	−27.47	−30.81	−43.07
	Theory	−6.10	−12.21	−18.31	−24.42	−30.52	−36.63
N_y	Exp.	−10.77	−19.31	−20.05	−30.44	−33.78	−41.58
	Theory	−5.91	−11.83	−17.74	−23.66	−29.57	−35.49
N_{xy}	Exp.	−7.71	−11.57	−20.58	−28.29	−33.44	−39.86
	Theory	−6.20	−12.40	−18.60	−24.80	−31.00	−37.20
N_1	Exp.	0.47	−3.43	0.53	−0.63	1.17	−2.45
	Theory	0.19	0.38	0.57	0.76	0.95	1.14
N_2	Exp.	−16.06	−27.75	−40.62	−57.29	−65.77	−82.19
	Theory	−12.21	−24.42	−36.63	−48.84	−61.05	−73.27

Table 8 Experiment and theoretical results for specimen with 9 cm rise at location II

		Load (N)					
Strain (cm/cm)		1110	2230	3340	4450	5560	6680
$\epsilon_x \times 10^6$		−4.00	−8.50	−13.00	−17.00	−21.00	−26.00
$\epsilon_y \times 10^6$		−2.67	−7.83	−11.67	−15.67	−19.67	−23.33
$\epsilon_{xy} \times 10^6$		6.93	13.86	20.78	27.71	34.64	41.57
		Force per unit length (N/cm)					
N_x	Exp.	−25.25	−56.06	−85.39	−112.11	−138.85	−170.78
	Theory	−23.84	−47.71	−71.56	−95.42	−119.27	−143.13
N_y	Exp.	−19.31	−53.09	−79.45	−106.18	−132.91	−158.90
	Theory	−23.51	−47.04	−70.55	−94.08	−117.59	−141.12
N_{xy}	Exp.	−15.43	−30.87	−46.30	−61.73	−77.17	−92.60
	Theory	−16.95	−33.92	−50.87	−67.83	−84.78	−101.75
N_1	Exp.	−6.56	−23.67	−36.03	−47.34	−58.66	−72.05
	Theory	−6.73	−13.46	−20.18	−26.91	−33.64	−40.37
N_2	Exp.	−37.99	−85.47	−128.81	−170.95	−213.09	−257.62
	Theory	−40.63	−81.29	−121.92	−162.59	−203.21	−243.88

Table 9 Experiment and theoretical results for specimen with 9 cm rise at location III

		Load (N)					
Strain (cm/cm)		1110	2230	3340	4450	5560	6680
$\epsilon_x \times 10^6$		−11.50	−21.00	−33.00	−44.50	−56.00	−67.50
$\epsilon_y \times 10^6$		−12.83	−22.33	−32.00	−43.83	−53.67	−66.17
$\epsilon_{xy} \times 10^6$		1.15	4.62	9.81	11.55	12.12	17.32
		Force per unit length (N/cm)					
N_x	Exp.	−78.33	−141.82	−219.41	−296.63	−371.62	−449.58
	Theory	−64.20	−128.46	−192.66	−256.92	−321.12	−385.37
N_y	Exp.	−84.27	−147.76	−214.95	−293.66	−361.23	−443.64
	Theory	−64.05	−128.16	−192.21	−256.32	−320.37	−384.48
N_{xy}	Exp.	−2.57	−10.29	−21.87	−25.72	−27.01	−38.58
	Theory	−7.55	−15.12	−22.67	−30.23	−37.79	−45.35
N_1	Exp.	−77.37	−134.08	−195.21	−269.38	−338.92	−407.91
	Theory	−56.57	−113.19	−169.76	−226.38	−282.95	−339.57
N_2	Exp.	−85.23	−155.50	−239.16	−320.90	−393.92	−485.31
	Theory	−71.68	−143.43	−215.11	−286.85	−358.53	−430.28

Table 10 Experiment and theoretical results for specimen with 6 cm rise at location I

		Load (N)					
Strain (cm/cm)		1110	2230	3340	4450	5560	6680
$\epsilon_x \times 10^6$		−1.00	−3.50	−5.50	−7.00	−8.50	−10.50
$\epsilon_y \times 10^6$		−2.00	−3.00	−5.00	−6.00	−7.50	−9.00
$\epsilon_{xy} \times 10^6$		−3.00	−5.50	−9.50	−13.00	−16.00	−20.50
		Force per unit length (N/cm)					
N_x	Exp.	−7.80	−22.84	−36.20	−45.66	−55.69	−68.50
	Theory	−9.33	−18.66	−27.99	−37.32	−46.65	−55.98
N_y	Exp.	−12.25	−20.60	−33.97	−41.21	−51.24	−61.81
	Theory	−9.24	−18.49	−27.74	−36.99	−46.23	−55.48
N_{xy}	Exp.	−6.69	−12.25	−21.16	−28.96	−35.64	−45.66
	Theory	−6.11	−12.23	−18.34	−24.46	−30.57	−36.69
N_1	Exp.	−2.98	−9.42	−13.89	−14.39	−17.75	−19.37
	Theory	−3.17	−6.35	−9.52	−12.69	−15.87	−19.04
N_2	Exp.	−17.07	−34.02	−56.28	−72.48	−89.17	−110.94
	Theory	−15.40	−30.81	−46.20	−61.61	−77.01	−92.42

Table 11 Experiment and theoretical results for specimen with 6 cm rise at location II

		Load (N)					
Strain (cm/cm)		1110	2230	3340	4450	5560	6680
$\epsilon_x \times 10^6$		-5.00	-10.50	-15.00	-20.00	-25.00	-29.50
$\epsilon_y \times 10^6$		-5.67	-10.17	-15.67	-21.33	-26.67	-32.17
$\epsilon_{xy} \times 10^6$		3.46	9.81	16.17	20.78	24.83	31.18
		Force per unit length (N/cm)					
N_x	Exp.	-34.16	-69.80	-100.98	-135.14	-168.92	-200.10
	Theory	-34.76	-69.55	-104.30	-139.09	-173.85	-208.64
N_y	Exp.	-37.13	-68.31	-103.95	-141.08	-176.34	-211.98
	Theory	-34.64	-69.31	-103.96	-138.63	-173.27	-207.94
N_{xy}	Exp.	-7.71	-21.87	-36.01	-46.30	-55.30	-69.44
	Theory	-13.03	-26.07	-39.10	-52.14	-65.17	-78.21
N_1	Exp.	-27.79	-47.18	-66.43	-91.71	-117.21	-136.35
	Theory	-21.67	-43.36	-65.03	-86.72	-108.39	-130.08
N_2	Exp.	-43.49	-90.93	-138.50	-184.50	-228.05	-275.75
	Theory	-47.73	-95.50	-143.23	-191.00	-238.73	-286.50

Table 12 Experiment and theoretical results for specimen with 6 cm rise at location III

		Load (N)					
Strain (cm/cm)		1110	2230	3340	4450	5560	6680
$\epsilon_x \times 10^6$		-12.00	-22.00	-33.50	-44.00	-55.00	-65.50
$\epsilon_y \times 10^6$		-10.00	-24.00	-34.17	-46.00	-58.00	-67.17
$\epsilon_{xy} \times 10^6$		4.62	5.77	9.24	12.70	16.74	22.52
		Force per unit length (N/cm)					
N_x	Exp.	-77.97	-149.24	-224.61	-296.25	-370.88	-439.56
	Theory	-69.12	-138.31	-207.43	-276.62	-345.74	-414.92
N_y	Exp.	-69.06	-158.15	-227.58	-305.16	-384.24	-446.99
	Theory	-69.07	-138.19	-207.26	-276.39	-345.45	-414.58
N_{xy}	Exp.	-10.29	-12.86	-20.58	-28.29	-37.29	-50.16
	Theory	-5.33	-10.67	-16.01	-21.35	-26.68	-32.02
N_1	Exp.	-62.29	-140.09	-205.46	-272.07	-339.67	-392.98
	Theory	-63.76	-127.58	-191.34	-255.14	-318.91	-382.73
N_2	Exp.	-84.72	-167.31	-246.72	-329.35	-415.45	-493.57
	Theory	-74.43	-148.92	-223.35	-297.85	-372.27	-446.77

Table 13 Measured deflections for specimen with 6 cm rise along sections A–A and B–B for a load of 10 kN

			Deflection (cm)		
Gauge No.	*X*-coord. cm	*Y*-coord. cm	S611 (Reinf. Type I)	S621 (Reinf. Type II)	S631 (Reinf. Type III)
1	10	50	0.006	0.004	0.004
2	20	50	0.012	0.010	0.010
3	30	50	0.026	0.024	0.025
4	40	50	0.048	0.045	0.046
5	10	10	0.000	0.000	0.000
6	21	21	0.006	0.005	0.004
7	32	32	0.020	0.016	0.018
8	35	35	0.022	0.020	0.020
9	42.5	42.5	0.042	0.038	0.040
10	44	44	0.044	0.042	0.042

load, and progressively propagated to the corners along the diagonals. Before forming the failure mechanism, cracks were developed parallel to the supports, as shown in *Figure 15*. For shells with no surface reinforcement, failure occurred abruptly, even though they followed the same pattern of cracks as described previously (see *Figure 16*).

To establish a relationship between crack and failure loads to the rise of shells, respectively, two sets of curves were constructed, as shown in *Figures 17* and *18*. These figures show that, in most cases, the correlation can be described through a linear approximation. The curves furthermore show that a shell with wire mesh reinforcement

Table 14 Measured deflections for specimen with 9 cm rise along sections A–A and B–B for a load of 10 kN

Gauge No.	*X*-coord. cm	*Y*-coord. cm	Deflection (cm) S911 (Reinf. Type I)	S921 (Reinf. Type II)	S931 (Reinf. Type III)
1	10	50	0.000	0.000	0.000
2	20	50	0.008	0.003	0.004
3	30	50	0.014	0.012	0.012
4	40	50	0.032	0.030	0.030
5	10	10	0.000	0.002	0.002
6	21	21	0.006	0.004	0.004
7	32	32	0.014	0.012	0.012
8	25	25	0.006	0.003	0.004
9	42.5	42.5	0.038	0.031	0.033
10	44	44	0.038	0.034	0.036

Table 15 Failure load for tested shells (thickness = 3 cm = 1.18 in, Type I reinforcement)

Specimen designation	Rise (cm)	Initial crack load (lb)	Initial crack load (kN)	Ultimate load (lb)	Ultimate load (kN)
S511	5	1620	7.21	1850	8.23
S512	5	1732	7.71	1920	8.54
S513	5	1400	6.23	1980	8.81
S611	6	1428	6.35	2100	9.35
S612	6	—	—	2100	9.35
S613	6	1954	8.70	2220	9.88
S711	7	1992	8.86	2450	10.90
S712	7	2230	9.92	2480	11.04
S713	7	2200	9.79	—	—
S811	8	—	—	2520	11.21
S812	8	2260	10.06	2510	11.17
S813	8	2270	10.10	2570	11.44
S911	9	2430	10.81	2700	12.02
S912	9	2300	10.24	2680	11.93
S913	9	2450	10.90	2800	12.46

Table 16 Failure load for tested shells (thickness = 3 cm = 1.18 in, Type II reinforcement)

Specimen designation	Rise (cm)	Initial crack load (lb)	Initial crack load (kN)	Ultimate load (lb)	Ultimate load (kN)
S521	5	2230	9.92	2600	11.57
S522	5	2072	9.22	2590	11.53
S523	5	—	—	2670	11.88
S621	6	—	—	3072	13.67
S622	6	2690	11.97	3100	13.80
S623	6	2900	12.91	3233	14.39
S721	7	3000	13.35	3480	15.49
S722	7	3100	13.80	3550	15.80
S723	7	3180	14.15	—	—
S821	8	3820	17.00	4380	19.49
S822	8	4300	19.14	4500	20.03
S823	8	—	—	4480	19.94
S921	9	4500	20.03	5200	23.14
S922	9	4620	20.56	5280	23.50
S923	9	4800	21.36	—	—

Table 17 Failure load for tested shells (thickness = 3 cm = 1.18 in, Type III reinforcement)

Specimen designation	Rise (cm)	Initial crack load		Ultimate load	
		(lb)	(kN)	(lb)	(kN)
S531	5	1620	7.21	2310	10.28
S532	5	1810	8.05	2420	10.77
S533	5	—	—	2400	10.68
S631	6	1860	8.28	2600	11.57
S632	6	1800	8.01	2600	11.57
S633	6	—	—	2680	11.93
S731	7	1660	7.39	2760	12.28
S732	7	2100	9.35	—	—
S733	7	2150	9.57	2800	12.46
S831	8	—	—	3010	13.39
S832	8	2370	10.55	3000	13.35
S833	8	2450	10.90	3050	13.57
S931	9	—	—	3150	14.02
S932	9	2700	12.02	3200	14.24
S933	9	—	—	3280	14.60

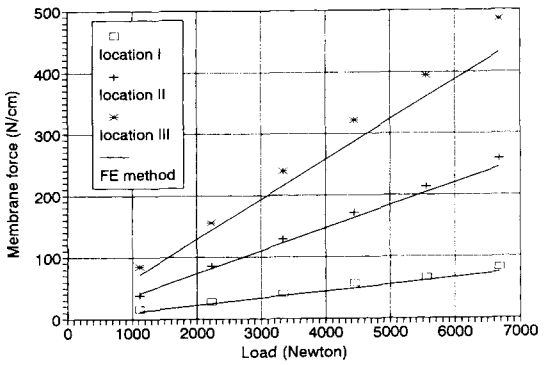

Figure 9 Principle membrane forces (rise = 9 cm)

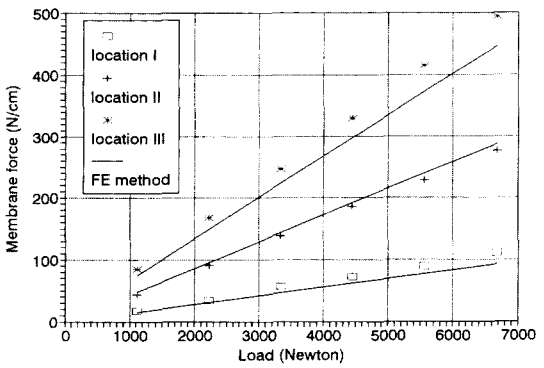

Figure 10 Principle membrane forces (rise = 6 cm)

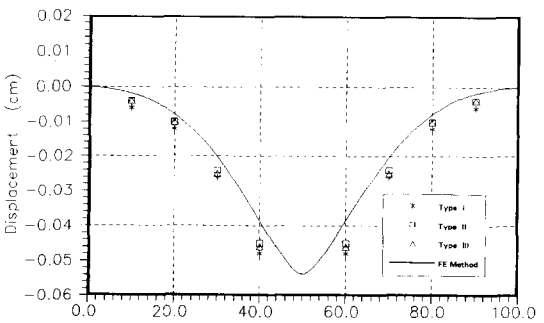

Figure 11 Displacement along section A–A for shell with 6 cm rise, 10 kN load

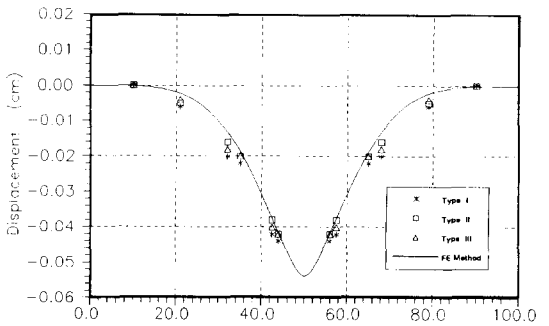

Figure 12 Displacement along section B–B for shell with 6 cm rise, 10 kN load

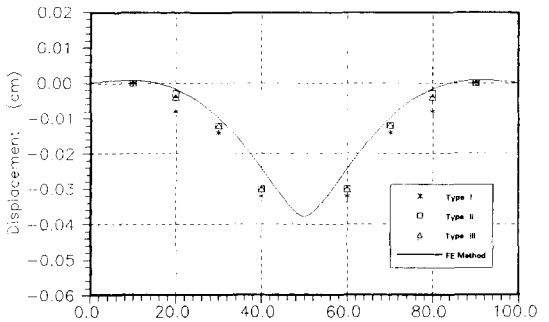

Figure 13 Displacement along section A–A for shell with 9 cm rise, 10 kN load

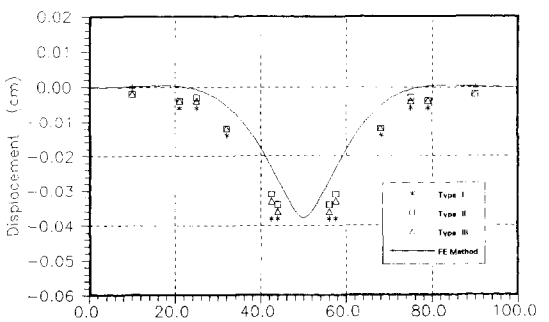

Figure 14 Displacement along section B–B for shell with 9 cm rise, 10 kN load

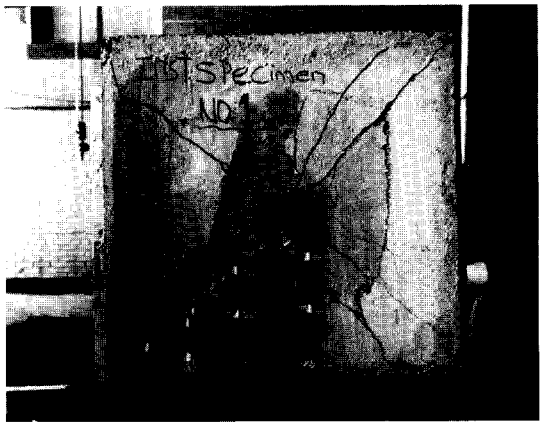

Figure 15 Crack patterns in a typical shell

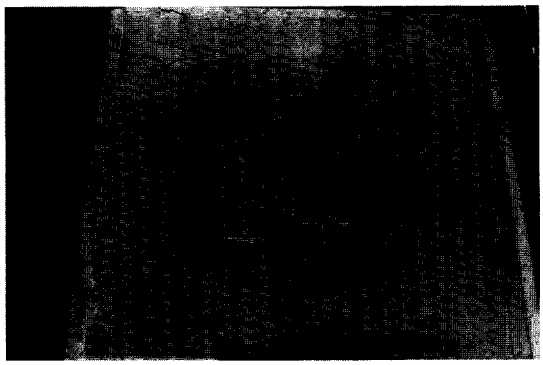

Figure 16 Failure mode of tested shells

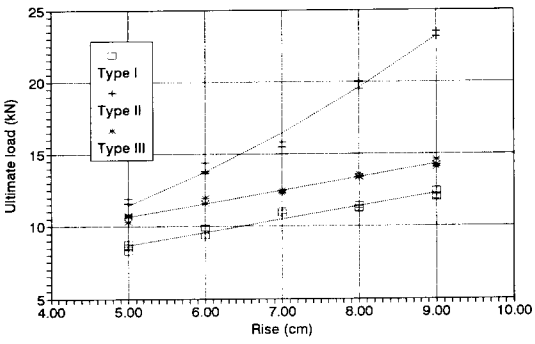

Figure 17 Variation of the ultimate load with rise

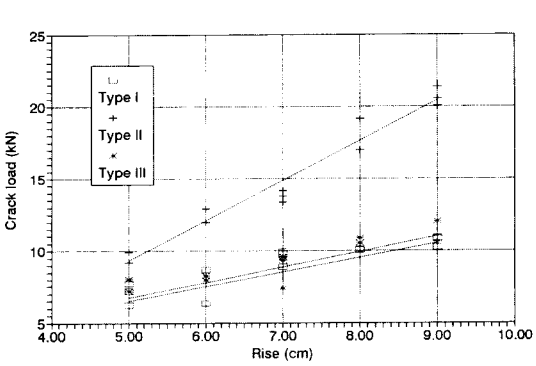

Figure 18 Variation of the crack load with rise

cracked at significantly higher loads than a shell with any other type of reinforcement (Types I and III). This is attributed to the more elastic behavior of shells, due to the presence of reinforcement. The following formulae described a best fit linear equation for experimental data in each case of crack and ultimate loads as designated in Case I and Case II, respectively.

Case I (crack load)

Type I $P_{cr} = 1.425 + 1.064R$
Type II $P_{cr} = -4.525 + 2.772R$
Type III $P_{cr} = 1.512 + 1.001R$

Case II (ultimate load)

Type I $P_u = 4.214 + 0.895R$
Type II $P_u = 6.192 + 0.2095R^2$
Type III $P_u = 6.056 + 0.916R$

where P_{cr} = crack load in kN; P_u = ultimate (failure) load in kN; R = rise in cm.

The experimental results presented in the paper pertain to the size of specimens chosen in the study, which has a potential for application to industrial use. However, the exact nature of behavioural response of larger dimension shells is a topic for further investigation.

Acknowledgments

We gratefully acknowledge the support given to this project by the Department of Civil and Environmental Engineering, Washington State University, Pullman, WA, USA and The Office of the Vice-Chancellor for Research, Sharif University of Technology, Tehran, I.R. Iran.

References

1 Vafai, A. and Farshad, M. 'Theoretical and experimental study of prefabricated funicular shell units', *Building and Environment* 1979, **14** (3), 209–216
2 Farshad, M. *Design and Analysis of Shell Structures*, Kluwer Academic Publishers, Dordrecht, Netherlands, 1992
3 Ramaswamy, G. S. 'Innovative applications of funicular shells', *IASS Symposium*, Osaka, Japan, 1986
4 Ramaswamy, G. S. *Design and Construction of Concrete Shell Roofs*, McGraw-Hill, New York, 1968
5 Vafai, A. and Farshad, M. 'Investigation of pointed domes; I. Theory', *Building and Environment* 1976, **11** (2), 81–85
6 Vafai, A. and Farshad, M. 'Investigation of pointed domes, II. Experiment', *Building and Environment* 1976, **11** (2), 87–90
7 Weber, J. W., Wu, K. and Vafai, A. 'Ultimate loads for shallow funicular concrete shells', *Northwest Science* 1984, **58** (3)
8 Elangoven, S. 'Analysis of funicular shells by the isoparametric finite element', *Computers and Structures* 1990, **34** (2), 303–311
9 Rajasekaran, S. and Sujatha, P. 'Configuration of deep funicular shells by boundary integral element method', *Computers and Structures* 1992, **44** (1/2), 213–221
10 Tessler, A. and Spiridigliozzi, L. 'Resolving membrane and shear locking phenomena in curved shear-deformable axisymetric shell elements', *International Journal of Numerical Methods in Enginering* 1988, **26**, 1071–1086
11 Habibullah, A. and Wilson, E. L. *SAP90 User's Guide*, Computers and Structures, Inc. Berkeley, California, 1989